IEEE Photonics Journal
An IEEE Photonics Society Publication

Optical Tunneling to Improve Light Extraction in Quantum Dot and Perovskite Light-Emitting Diodes

Volume 12, Number 6, December 2020

Guanding Mei
Dan Wu
Shihao Ding
Wallace C. H. Choy
Kai Wang
Xiao Wei Sun

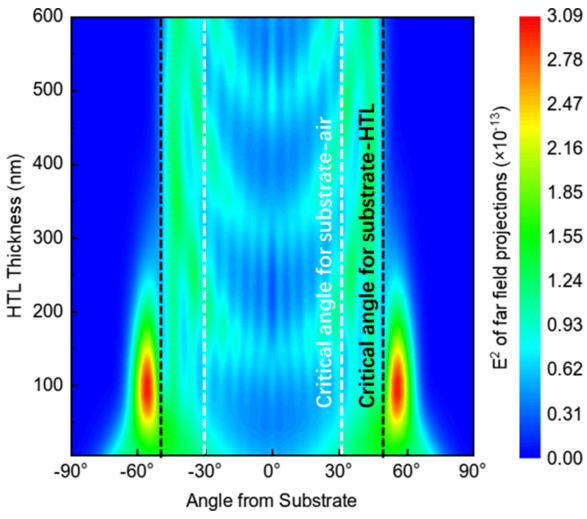

DOI: 10.1109/JPHOT.2020.3038275

Optical Tunneling to Improve Light Extraction in Quantum Dot and Perovskite Light-Emitting Diodes

Guanding Mei,[1] Dan Wu,[1] Shihao Ding,[1,2] Wallace C. H. Choy,[3] Kai Wang [1], and Xiao Wei Sun [1,2,4]

[1]Guangdong University Key Lab for Advanced Quantum Dot Displays and Lighting, Shenzhen Key Laboratory for Advanced Quantum Dot Displays and Lighting, Department of Electrical and Electronic Engineering, Southern University of Science and Technology, Shenzhen 518055, China
[2]Shenzhen Planck Innovation Technologies Company Ltd, Shenzhen 518112, China
[3]Department of Electrical and Electronic Engineering, The University of Hong Kong, Hong Kong 999077, China
[4]Key Laboratory of Energy Conversion and Storage Technologies (Southern University of Science and Technology), Ministry of Education, Shenzhen 518055, China

DOI:10.1109/JPHOT.2020.3038275

Manuscript received October 31, 2020; accepted November 9, 2020. Date of publication November 16, 2020; date of current version December 4, 2020. This work was supported in part by the National Key Research and Development Program of China administrated by the Ministry of Science and Technology of China under Grants 2016YFB0401702 and 2017YFE0120400, in part by the National Natural Science Foundation of China under Grants 61674074, 61875082, and 61405089, in part by Key-Area Research and Development Program of Guangdong Province under Grant 2019B010925001, in part by the Guangdong University Key Laboratory for Advanced Quantum Dot Displays and Lighting under Grant 2017KSYS007, in part by the Distinguished Young Scholar of Natural Science Foundation of Guangdong under Grant 2017B030306010, in part by the Shenzhen Key Laboratory for Advanced Quantum Dot Displays and Lighting (No. ZDSYS201707281632549, and in part by Shenzhen Peacock Team Project under Grant KQTD2016030111203005). Corresponding author: Xiao Wei Sun (e-mail: sunxw@sustech.edu.cn).

Abstract: An effective strategy based on optical tunneling is developed to significantly improve the efficiency of quantum dots light-emitting diodes (QLEDs) and perovskite light-emitting diodes (PeLEDs). Contrary to the common impression that the hole transport layers (HTL) with low refractive index will severely confine lights according to Snell's law, optical tunneling unlocks a channel to extract the lights through HTL. In this work, we demonstrate the light beyond the critical angle still has a chance to penetrate into the substrate and finally emit outside the device. An optical tunneling model is also presented here to quantitatively describe the light extraction through optical tunneling and reveal related factors. Applying a thin HTL (thickness = 10 nm) and a high-index substrate (refractive index = 2) in the typical device architecture (Glass/ITO/PEDOT:PSS/EML/TPBi/LiF/Al), substrate modes can be improved from 18% to 60%. Therefore, optical tunneling followed by EES is believed to be a cost-effective strategy to enhance light extraction efficiency. This work unravels the potential to further significantly improve the efficiency of QLEDs and PeLEDs.

Index Terms: Optical tunneling, light extraction efficiency, quantum dot light-emitting diodes, perovskite light-emitting diodes.

1. Introduction

Being considered as one of the next-generation display technologies, quantum-dot light-emitting diodes [1] (QLEDs) and perovskite light-emitting diodes [2] (PeLEDs) have attracted great attention recently. These LEDs show impressive efficiencies and narrow electroluminescent spectra, which allow energy-efficient lighting and wide color gamut display. The external quantum efficiencies (EQE) of QLEDs and PeLEDs have reached 20% [3], [4] for devices with flat substrates, which is the theoretical limit considering them as an analogy of organic light-emitting diodes (OLEDs). The EQE is defined as:

$$\mathrm{EQE} = IQE \times LEE \tag{1}$$

where IQE is internal quantum efficiency determined by optical and electrical properties of materials, LEE is light extraction efficiency or light out-coupling efficiency, which specifies the ratio of the photons escaped from the LED to all photons emitted from the active region [5].

So far, IQE has reached its limit for QLEDs and PeLEDs as reported in the literatures [6], [7], the LEE thus becomes the dominant factor restricting EQE. A typical LED architecture is plotted in Fig. 1(a), reflection and refraction happened at the interface of each layer. Snell's law tells us that LEE is mainly determined by the refractive index of emitting layer (EML). In visible spectrum, common organic polymers as EML in organic light-emitting diodes (OLEDs) have a refractive index of 1.7-1.8 [8], neat CdSe/CdS core/shell QD films as EML in QLEDs have refractive indices of 1.8-2 [9], and the refractive indices of $CH_3NH_3PbI_3$, $CH_3NH_3PbBr_3$, $CH_3NH_3PbCl_3$, and $CsPbI_3$ perovskites as EML in PeLEDs are 2.2-3.2 [10], [11], 2.0-2.5 [12], [13], 2.0-2.4 [14], and 2.3-2.5 [15] respectively. High refractive indices of quantum dots and perovskite lead us to reexamine the LEE limit for QLEDs/PeLEDs.

According to Snell's law, reflection and refraction are determined by index difference between layers. It follows a crude approximation [16] for LEE calculations, LEE $= 1/(2n^2)$, where **n** is the refractive index of EML. Since the $1/(2n^2)$ model assumes Lambertian approximation neglecting interference effects, absorption and re-absorption. It is also possible to discard Lambertian approximation then calculate LEE directly by Eq. (2) [orange dashed line in Fig. 1(b)] according to Snell's law.

$$LEE = 1 - \sqrt{1 - \left(\frac{{n_{Air}}^2}{{n_{EML}}^2}\right)} \tag{2}$$

where $\boldsymbol{n_{Air}}$ is the refractive index of air ($\boldsymbol{n_{Air} = 1}$), $\boldsymbol{n_{EML}}$ is the refractive index of EML.

As shown in Fig. 1(b), Under the assumption of $1/(2n^2)$ model, LEE is highly related to the index of EML. The theoretical LEE limits of QLEDs are from 16% to 13%, and that of PeLEDs are from 13% to 5%, instead of the constant 20% as some articles [6], [17]–[19] reported. Although some articles state that photon recycling in PeLED may assist with optical outcoupling, from the perspective of light extraction, the severe LEE limits are still the major problem for the optimization of QLEDs and PeLEDs.

The LEE limit problem destined us to evaluate power dissipation and develop a relatively cost-effective light extraction strategy. Fortunately, the light extraction strategies in OLEDs provide a lot of references for QLEDs and PeLEDs to improve LEE, e.g., high-index substrates [20], microlens array [21], [22], scattering films [23], [24], embedded low-index grids [25], low-index electron transport layer [8] (ETL), nanophotonic substrate [26]. To find the effective light extraction strategy for QLEDs and PeLEDs, power dissipation coupled to different optical channels must be analyzed. Herein, two major optical channels are introduced: substrate modes mean that the photons are trapped within the substrate by total internal reflection (TIR) at the interface between air and the substrate; waveguide modes mean the photons are trapped by TIR at electrodes, hole and electron transport layers and EML.

Compared with OLEDs, it is obvious that higher EML refractive indices of QLEDs and PeLEDs bring stronger TIR at the interface between EML and the hole transport layer (HTL) according to Snell's law. Some commonly used HTL have a refractive index smaller than EML, e.g., PEDOT:PSS

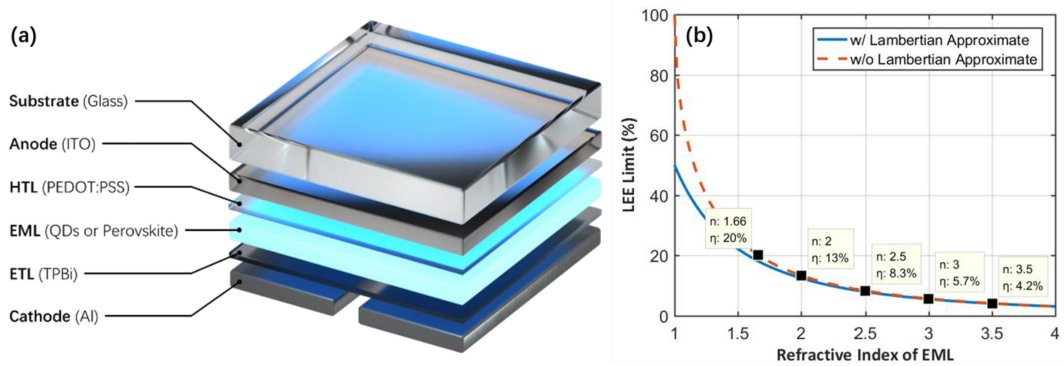

Fig. 1. (a) Typical QLED and PeLED structure. (b) LEE (η) with refractive index ($\boldsymbol{n}$) of EML neglecting interference effects and absorption.

[27] ~1.52, PVK [28], [29] ~1.7, TFB [30] 1.6-2.0, Spiro-OMeTAD [31] 1.6-1.9, P3HT [32] 1.6-2.2 (for the chemical information, please refer to the corresponding references). In this study, we take PEDOT:PSS as HTL for illustration, i.e., $\boldsymbol{n}_{HTL} = 1.52$.

Borrowing the crude approximation of Eq. (2), when the EML ($CH_3NH_3PbBr_3$) has the refractive index of 2, and the HTL (PEDOT:PSS) has the refractive index of 1.5, we replace $\boldsymbol{n}_{Air}$ with $\boldsymbol{n}_{HTL}$ in Eq. (2) to estimate the proportion of lights that can enter HTL, which is 33.8%. Thus, 66.2% of the lights will be reflected by the HTL before they propagated to the substrate, which means most of photons were trapped in EML (belongs to waveguide modes) instead of the substrate (substrate modes). Since most photons were trapped in waveguide modes, we naturally think of using the internal extraction structure (IES), where light extraction structure is inserted into the device except substrate-air boundary, to disrupt waveguide modes. Some internal extraction structures [19], [26], [33], [34] have been proven to improve LEE effectively.

However, from the perspective of electromagnetics, these lights with incidence angle greater than the critical angle are not necessarily limited by TIR. Snell's law only concludes that the lights beyond the critical angle are totally reflected by HTL, but it does not account for evanescent waves due to the nanoscale thickness of HTL in QLEDs and PeLEDs. As the simulated time-domain electric field evolution and the schematic shown in Fig. 2, when the incident angle of the plane wave in EML larger than critical angle θ_c, evanescent waves [35] were formed at the interface and propagates parallel to the interface [Fig. 2(b)], eventually reflected back to EML resulting in TIR [Fig. 2(c)]. The electric field of evanescent waves decays exponentially away from the interface, hence the energy is concentrated close to the interface. The penetration depth of the evanescent wave, in which the field of the evanescent wave decay to $e^{-1} = 36.8\%$ is defined as:

$$Penetration\ depth = \frac{\lambda}{2\pi n_2 \times \sqrt{\left(\frac{n_1}{n_2}\right)^2 \sin^2\theta_i - 1}} \tag{3}$$

where λ is the free-space wavelength, θ_i is the incident angle, $\boldsymbol{n_1}$ is the refractive index of EML, $\boldsymbol{n_2}$ is the refractive index of HTL.

By substituting $\lambda = 530$ nm, $\boldsymbol{n_1} = 2$, $\boldsymbol{n_2} = 1.5$ into Eq. (3), when $\theta_i = 50°$, the penetration depth = 270.4 nm; when $\theta_i = 60°$, the penetration depth = 97.4 nm. Fortunately, for QLEDs and PeLEDs, the HTL thickness is usually thinner than 100 nm. As shown in Fig. 2(h), evanescent waves can meet the ITO layer before their amplitude decay to near zero. Meanwhile, the refractive index $\boldsymbol{n_3}$ of ITO [36] is 1.8-2.2 in visible spectra, which is higher than that of HTL. Fig. 2(e)–(g) show that a portion of the evanescent waves formed in HTL was refracted into the ITO layer, while the other portion of the waves were reflected, resulting in frustrated total internal reflection (FTIR)[37]. This phenomenon is also called optical tunneling.

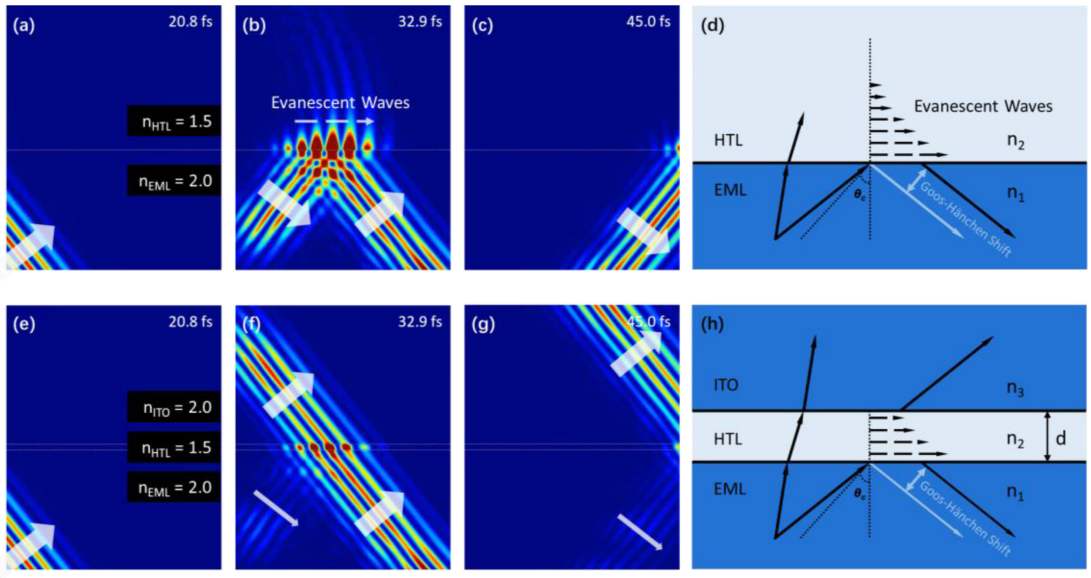

Fig. 2. (a)–(c) Time-domain E field evolution of total internal reflection. (d) Total internal reflection with thick HTL. (e)–(g) Time-domain E field evolution of optical tunneling. (h) Optical tunneling with thin HTL.

Optical tunneling shows the propagation of light beyond the critical angle where a thin low refractive index media is surrounded by two high-index media. Because optical tunneling provides a channel to extract light from EML to the ITO layer then to the substrate, we can conveniently arrange extraction structures on the substrate to extract light into the air. In this study, we aim to verify the existence of optical tunneling in QLEDs and PeLEDs, as well as to evaluate the impact of optical tunneling on the optical energy distribution in the LEDs, hopefully to shed light on the light extraction design for QLEDs and PeLEDs.

2. Optical Tunneling Analysis

To confirm that optical tunneling exists in a specific structure of LEDs, the finite-difference time-domain (FDTD) method based on Maxwell's solver is a reliable simulation method. Here we take the PeLED as an example, the conclusion can be extended to QLEDs in general. A typical device architecture (Glass/ITO/PEDOT:PSS/EML/TPBi/LiF/Al) of the planar structure PeLED[[38], [39] is plotted in Fig. 3(a) with refractive index ***n*** and thickness ***d***. An electromagnetic point dipole source is located in the middle of EML with center wavelength of 530 nm and wavelength span of 200 nm, and the orientation of the dipole source is swept along the x, y and z axes and then sum up to achieve the isotropic dipole emitter. A far-field monitor [white dashed line Fig. 3(a)] is placed within the substrate to collect the transmittance in the glass (the ratio of the intensity of the light transmitted into the glass to that of the incident light in EML).

According to the exponential attenuation of the evanescent wave field, HTL thickness is a significant parameter expected to enhance optical tunneling. The refractive index of glass is set to 1.95 (the same with ITO), the far-field E^2 intensity $(V\ m^{-1})^2$ angular distribution plotted in Fig. 3(b) is collected by the monitor [white dashed line Fig. 3(a)] in the Lumerical FDTD Solutions. When HTL is thicker than 250 nm, lights beyond the critical angle of the substrate and HTL [black dashed line in Fig. 3(b)] hardly penetrate the HTL obstacle due to the limited penetration depth of the evanescent wave. Instead, as the thickness of HTL decreases to below 250 nm, the lights break the limitation of the critical angle then achieve a higher transmittance with the wider angular distribution.

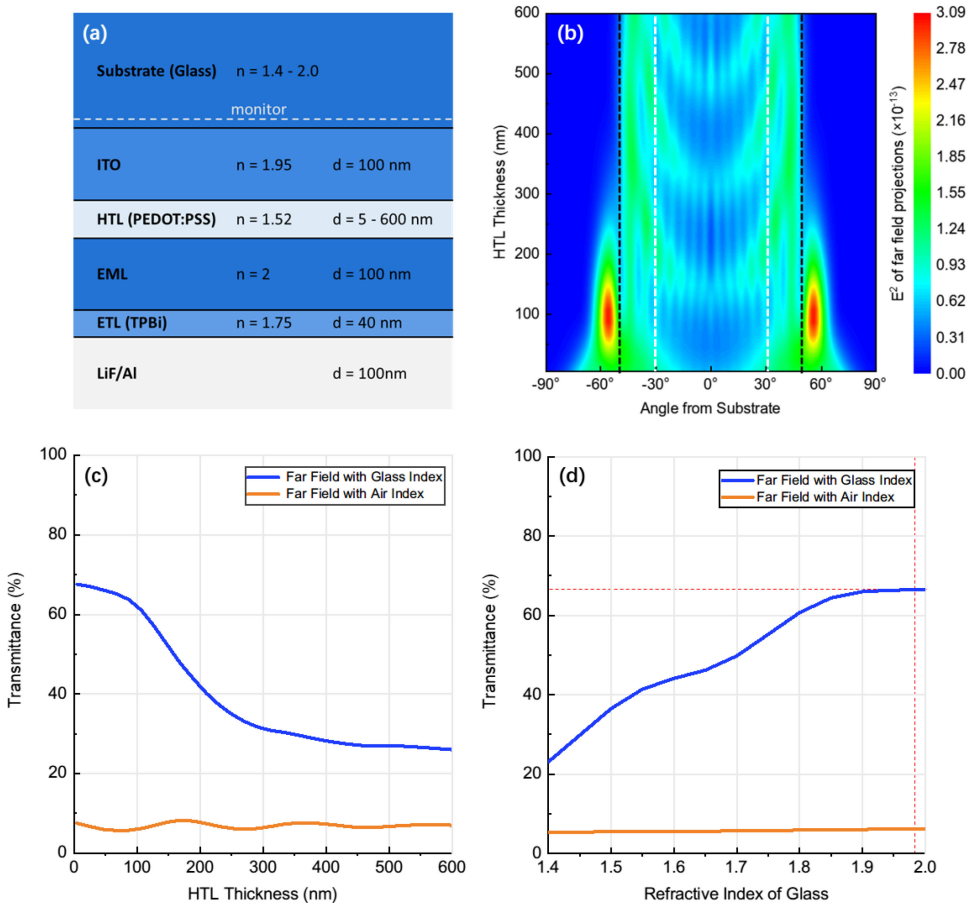

Fig. 3. (a) Device architecture of the planar structure QLED and PeLED. (b) Far-field E^2 intensity $(V\ m^{-1})^2$ angular distribution with varied HTL thicknesses in the glass. (c) Transmittance of far field as a function of HTL thickness. (d) Transmittance of far field as a function of the refractive index of the glass with HTL thickness of 50 nm.

The transmittance with varied HTL thicknesses is plotted in Fig. 3(c), as the thickness of the HTL decreases from 600 nm to 1 nm, the transmittance in the glass is greatly enhanced from 26% to 68%. Subtracting the light entering the air [orange line in Fig. 3(c)], we get that the substrate modes is improved from 18% to 60%. The transmittance increased faster as the HTL thickness decreases to within 100-300 nm, this is attributed to the exponential attenuation of the evanescent wave field. However, when the HTL thickness within 100 nm, the growth of transmittance becomes slower, which is not only due to the fact that the refractive indices of ITO and glass ($\boldsymbol{n}_{glass} = 1.95$) are still a little lower than EML ($n_{\mathrm{EML}} = 2$), but also to the error at large incident angle caused by the limited monitor size in the software. Fortunately, in most device structures, the HTL is designed within 100 nm for efficient charges injection.

The optical tunneling processes are revealed in the electric field evolution with time elapses for varied HTL thicknesses shown in Fig. 4(a)–(c). When HTL thickness is 50 nm [Fig. 4(a)], photons can penetrate into ITO with little reflections. When HTL thickness is 300 nm [Fig. 4(c)], at 10.40 fs, the evanescent waves travel near the interface between EML and HTL along the horizontal direction, its electric field decays to near zero before it meets the ITO; at 14.56 fs, the evanescent waves become reflected lights leading to TIR; after 18.82 fs, the evanescent waves are formed again then repeat this process, eventually dissipated in energy losses.

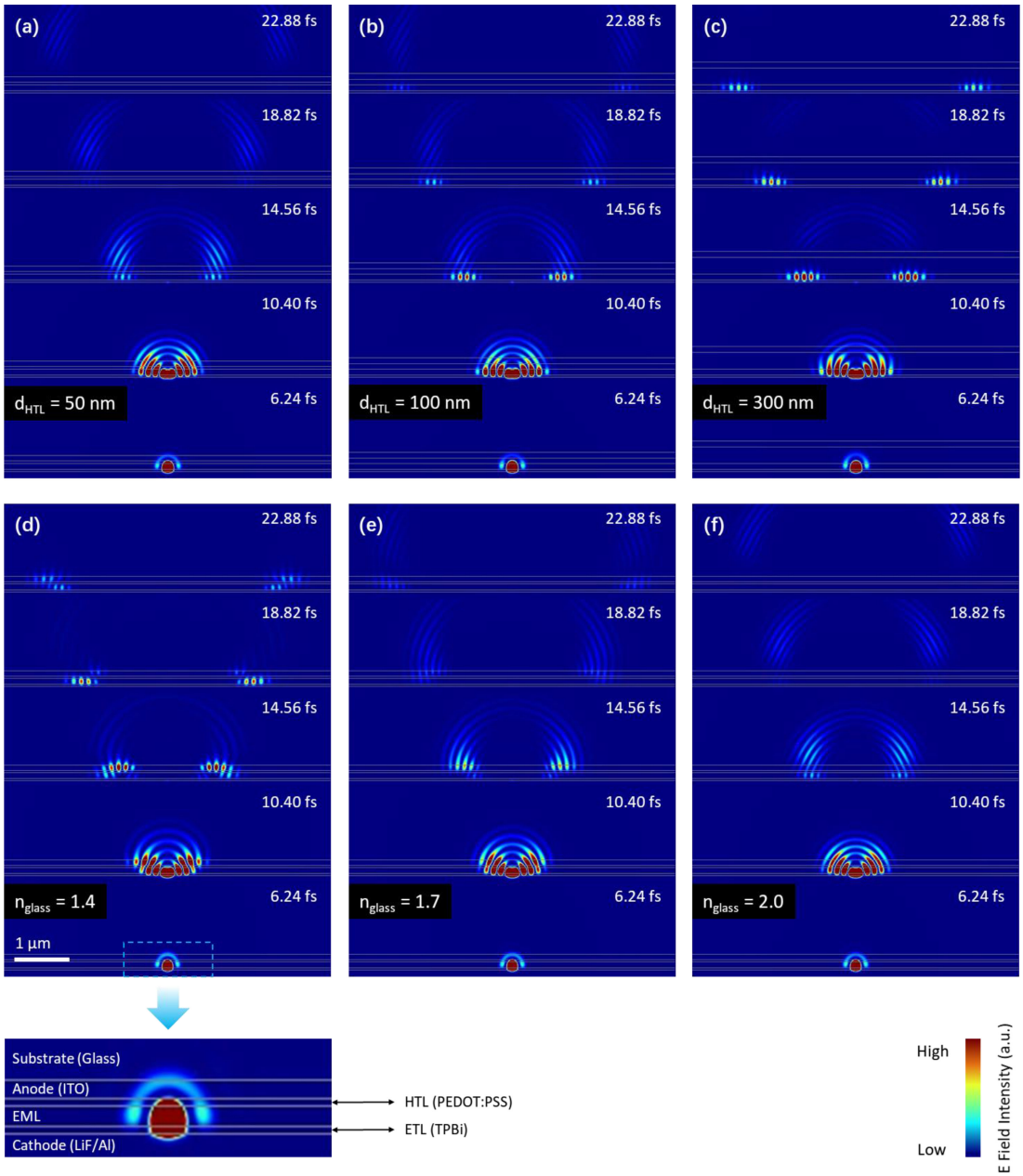

Fig. 4. Time domain E field evolution from 6.24 fs to 22.88 fs for (a) $d_{HTL} = 50$ nm, $n_{glass} = n_{ITO}$, (b) $d_{HTL} = 100$ nm, $n_{glass} = n_{ITO}$, (c) $d_{HTL} = 300$ nm, $n_{glass} = n_{ITO}$, (d) $d_{HTL} = 40$ nm, $n_{glass} = 1.4$, (e) $d_{HTL} = 40$ nm, $n_{glass} = 1.7$, (f) $d_{HTL} = 40$ nm, $n_{glass} = 2.0$.

During HTL thickness sweep above, the glass have the same refractive index as ITO (high-index glass), so that the light entering the ITO can completely enter the glass, thereby the separate role of HTL thickness in transmittance is investigated. If the refractive index of the glass decrease, the reflection on the interface between ITO and the glass will limit the transmittance.

To further transmit light into the glass, it is necessary to explore the relationship between the transmittance and the refractive index of glass. The refractive index of the glass is swept from 1.4 - 2.0 at the thickness of the HTL of 50 nm. The results [Fig. 3(d)] show that the higher refractive

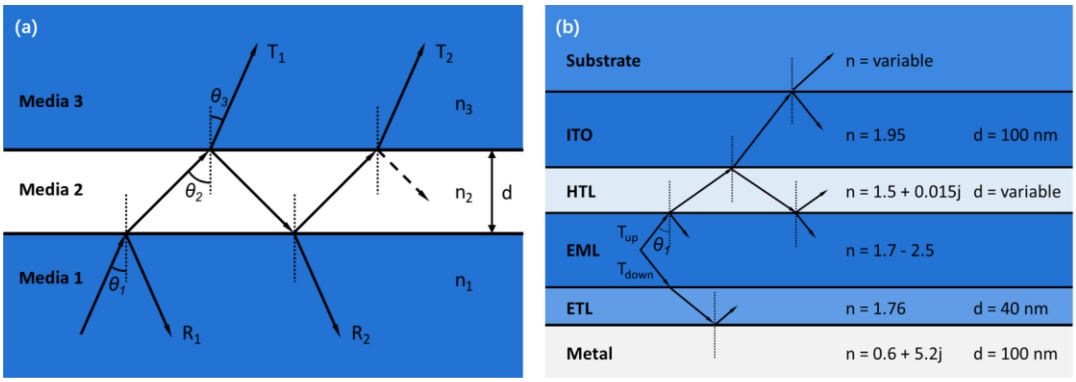

Fig. 5. (a) Multiple reflections in single layer. (b) Stack of QLEDs or PeLEDs.

index of glass brings stronger transmittance in the glass. If the refractive index of glass (substrate) is smaller than that of ITO, the photons enter the ITO layer through optical tunneling will still be reflected by the glass, so the proportion of lights can enter the glass is eventually determined by the refractive index of glass. As shown in Fig. 3(d), the transmittance saturates at $\boldsymbol{n}_{\mathbf{glass}} = \sim$1.95. Namely, the maximum effective refractive index of the glass is limited by the index of EML ($\boldsymbol{n}_{EML} =$ 2) and the index of ITO[36] ($\boldsymbol{n}_{ITO} =$ 1.95).

The E field evolution with time elapses for varied refractive indices of the substrate are summarized in Fig. 4(d)–(f). When a normal refractive index glass ($\boldsymbol{n}_{glass} =$ 1.4) is used [Fig. 4(d)], the transmitted waves by optical tunneling will be reflected by the substrate, then eventually dissipated in absorption loss. On the contrary, nearly all of photons propagated into ITO with the aid of optical tunneling can further escape into the high-index glass ($\boldsymbol{n}_{glass} =$ 2.0) as shown in Fig. 4(f).

As can be seen, to enhance the substrate modes, the thin HTL and high refractive index substrates are necessary due to optical tunneling. Although there are more photons entered into the substrate, LEE [i.e., far-field transmittance in the air, orange line in Fig. 3(c) and (d)] is not much improved. Because the lights beyond the escape cone [white dashed line in Fig. 3(b)] are still confined at the interface of glass and air.

3. Optical Tunneling Model

Since the FDTD method is based on Maxwell's equations, we can observe the obvious interference patterns in Fig. 3(b), these patterns are mainly caused by the microcavity effect, which is strongly related to the position of the dipole and the thickness of EML (the interference in the other layer also contributes to the intensity fluctuations, but not dominant). The microcavity effect affects our judgment on the independent effect of optical tunneling. To isolate the effect of optical tunneling, the interference in EML (microcavity effect) and other effects (e.g., near-field absorption, surface plasmon polariton, re-absorption) are neglected. Because the results we get from FDTD method (or Chance, Prock and Silbey (CPS) model[40]) are precise but comprehensive including multiple effects, which may be difficult for us to analyze whether the mode change is due to optical tunneling or microcavity effect. Therefore, an optical tunneling model based on the transfer-matrix method is presented here to illustrate how optical tunneling performs in a LED structure.

3.1 Transfer-Matrix Method

A ray through an interface will be partially transmitted and then partially reflected. As a layer surrounded by two semi-infinite media shown in Fig. 5(a), depending on the refractive index and thickness of the layer, the multiple reflections will lead to destructive or constructive interference.

Moreover, the multiple reflections mean that the overall transmittance and reflectance of the layer is the sum of an infinite number of transmissions and reflections. To solve the interference and sum of reflections of multilayer in LED, the transfer-matrix method[41] is more convenient and intuitive than solving Fresnel's equations recursively. Fig. 5(b) simply depicts multiple reflections in LED stack, the HTL and ITO can be treated as a single top layer under the transfer-matrix method, and ETL and metal are treated as a single bottom layer similarly. Herein, R_t, T_t, A_t and R_b, T_b, A_b represent the reflectance, transmittance, absorption of the top and bottom layers, respectively. The absorption can be derived from $A = 1 - (T + R)$ when absorbing materials are described using a complex refractive index ($\mathbf{n} + \mathbf{jk}$), where **k** is the extinction coefficient. For instance, the thicker PEDOT:PSS ($n = \mathbf{1.5} + \mathbf{0.015j}$) not only brings greater R_t as optical tunneling described, but also increase A_t due to absorption, which will further reduce T_t.

3.2 Three-Dimensional Model

Because lights travel in three-dimensional space, the optical tunneling model integrates the transmittance in the spherical coordinate system under some reasonable conditions and assumptions:

Source and Polarization. Since each photon created by spontaneous emission has a random direction, it is a consensus to use the isotropic point light source to simulate spontaneous emission in EML. In addition, as Fresnel's equations clarified, s and p polarization light propagate differently in the media. This model averages the transmittance of s and p polarization light, i.e., $\boldsymbol{T_0} = (\boldsymbol{T_s} + \boldsymbol{T_p})/2$.

Multiple Reflection. Multiple reflections from ETL and metal cathode make the photons failed in their first tunneling still have a second chance to participate in tunneling, so we must consider the reflection-assisted optical tunneling. The multiple reflection paths were represented in Fig. 5(b), since the interference in EML is neglected, each time the light is reflected back to EML from ETL and metal cathode with dissipation, the intensity of incident light I_0 becomes $R_b \times I_0$. Averaging transmittance of upward incident light (T_{up}) and downward incident light (T_{down}), the total transmittance (T_{total}) can be calculated by integrating recursive reflection:

$$T_{up} = T_t + T_t \times R_t \times R_b + T_t \times (R_t \times R_b)^2 + \ldots = \frac{T_t}{1 - R_t \times R_b} \tag{4}$$

$$T_{down} = \frac{R_b \times T_t}{1 - R_t \times R_b} \tag{5}$$

$$T_{total} = \frac{T_{up} + T_{down}}{2} = \frac{(1 + R_b) \times T_t}{2 \times (1 - R_t \times R_b)} \tag{6}$$

3.3 Results

The optical tunneling model is applied to the device structure shown in Fig. 5(b) with source wavelength of 530 nm. The thickness of HTL is swept from 0 to 500 nm. The relationship between the transmittance, incident angle, and HTL thickness was observed in Fig. 6.Fig. 6(a)–(c) shows that a normal glass of $\boldsymbol{n}_{glass} = 1.55$ is used as the substrate, the transmittance with the incident angle is slightly influenced by the thickness of HTL ($\boldsymbol{n}_{HTL} = 1.5$) [Fig. (6)], because the contribution of optical tunneling is reflected by the low-index substrate. If we substitute the index-matched substrate ($\boldsymbol{n}_{Sub} = \boldsymbol{n}_{EML}$) for the normal glass [Fig. 6(d)–(f)], the incident light beyond the critical angle at EML/HTL interface ($\theta_c = 63.4°$, $49.5°$, $37.4°$ for $\boldsymbol{n}_{EML} = 1.7$, 2.0, 2.5, respectively) also penetrated into the substrate [Fig. (6)], in this case, the total transmittance from EML to the substrate increases as the thickness of HTL decreases.

The increase of transmittance as HTL thickness decreases corresponds to the exponential attenuation of the evanescent wave field. Fig. 6 suggests that when the high-index substrate is used, reducing the HTL thickness can greatly increase the proportion of lights that can reach the substrate. Fortunately, the thickness of the HTL is usually within 100 nm. At present, it is possible to prepare the ultra-thin PEDOT: PSS with thickness of 7 nm [42] as the HTL, which will further

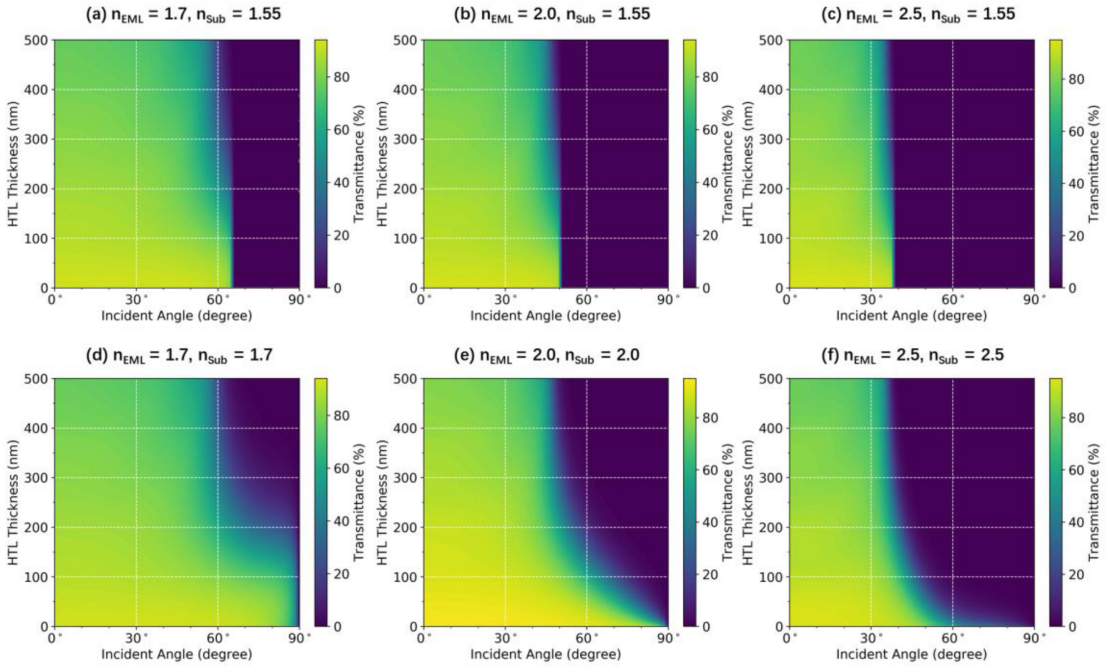

Fig. 6. Transmittance as a function of incident angle and HTL thickness for $\lambda = 530$ nm, and varied refractive indices of (a) $n_{EML} = 1.7$ $n_{Sub} = 1.55$, (b) $n_{EML} = 2$ $n_{Sub} = 1.55$, (c) $n_{EML} = 2.5$ $n_{Sub} = 1.55$, (d) $n_{EML} = 1.7$ $n_{Sub} = 1.7$, (e) $n_{EML} = 2.0$ $n_{Sub} = 2.0$, (f) $n_{EML} = 2.5$ $n_{Sub} = 2.5$.

enhance the lights entering the substrate. This suggests that reducing the thickness of the HTL is a simple and effective strategy to improve the transmittance from EML to the substrate.

Also note that, when we consider the total transmittance, it is the solid angle that the integral was computed over. Hence, the transmittance at a large angle contributes more to total transmittance than that at a small angle. Fig. 7 shows the total transmittance obtained by the integration. When high-index glass ($\boldsymbol{n_{glass}} = 2$) is used, although the angular distribution of transmitted lights only doubled as HTL thickness decrease in Fig. 6(e), the total transmittance quadrupled from 22% to 86% in Fig. 7(a). Meanwhile, the absorption loss also decreases with thinner HTL.

The dispersion of transmittance is shown in Fig. 7(b), where we used red (700 nm), green (530 nm), and blue (470 nm) light for the plot. It can be seen that the longer wavelength brings higher transmittance due to the greater penetration depth of evanescent wave [Eq. (2)]. Therefore, the optical tunneling is in a higher demand for blue light.

To explore the trend of optical tunneling when EML has a higher refractive index ($\boldsymbol{n_{EML} > 2}$), we assume the high-index substrate with $\boldsymbol{n_{Sub}}$ exceeds the refractive index of ITO ($\boldsymbol{n_{ITO} = \sim 2}$) is available. As the results shown in Fig. 6(f), the enhancement of transmittance by thinner HTL is not as strong as we expected, and the transmittance at $\boldsymbol{n_{EML}} = 2.5$ (purple line) in Fig. 7(c) is much lower than that at $\boldsymbol{n_{EML}} = 2.0$ (blue line) and $\boldsymbol{n_{EML}} = 1.7$ (cyan line). This phenomenon is due to ITO acted as an "optical barrier" when the index of ITO is lower than that of EML. In this case, the thickness of ITO also becomes an important factor for optical tunneling. As an assumption, if the ITO thickness is close to zero, the transmittance will increase sharply from 14% to 90% with the decrease in HTL thickness [Fig. 7(d)]. The enhancement is easy to understand from the intensity angular distribution with and without ITO [Fig. 8(c)–(d)], which will be discussed in Section 3. Consequently, when the refractive index of the EML is higher, the device has a stronger demand for the index-matched substrate and thinner HTL to compensate for the lower transmittance.

As described, the result of the optical tunneling model is consistent with what the FDTD method shows. The difference is that the optical tunneling model neglects the interference in EML and other

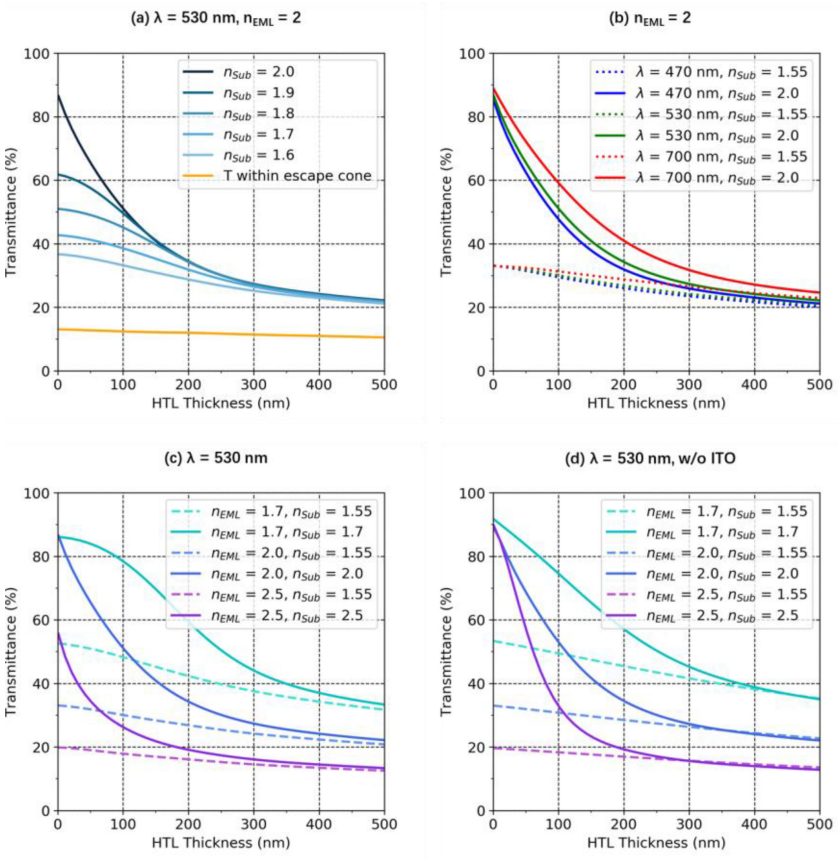

Fig. 7. Total transmittance from EML to the substrate as a function of HTL thickness when (a) $\lambda =$ 530 nm, $n_{EML} = 2$ (b) $n_{EML} = 2$, (c) $\lambda = 530$ nm, (d) $\lambda = 530$ nm without ITO.

loss effects, then provides an easy way to investigate the independent role of optical tunneling. We can think of the result of the optical tunneling model as a more general conclusion, but when analyzing multiple effects in a specific device, it is still recommended to apply the comprehensive models like FDTD method and CPS model.

4. Improving the Efficiency

Fig. 8 shows the emission intensity angular distribution within the substrate according to the optical tunneling model. Compared with HTL thickness of 300 nm (orange line in Fig. 8), the light intensity within the substrate at HTL thickness of 30 nm has a wider angular distribution (blue line in Fig. 8) due to optical tunneling. According to Snell's law, only lights contained in the escape cone (dashed magenta line in Fig. 8) have a chance to escape to air, while the light penetrated with the help of optical tunneling cannot escape to air directly, thus optical tunneling in a planar structure has no direct enhancement on LEE [yellow line in Fig. 7(a)]. Calculating the ratio of the transmittance within the escape cone to the transmittance in the substrate when HTL thickness $=$ 30 nm in Fig. 7(a), it is observed that only about 16% of lights in the substrate can escape to air, a large proportion of light outside escape cone is dissipated. This indicates that optical tunneling provides a large potential for LEE improvement, the only thing needs to be done is to extract these lights from the substrate.

To extract this part of the lights from the substrate to air, thus contributing to the useful radiation, the external light extraction structure (EES) on the substrate is sufficient. Fortunately, a lot of

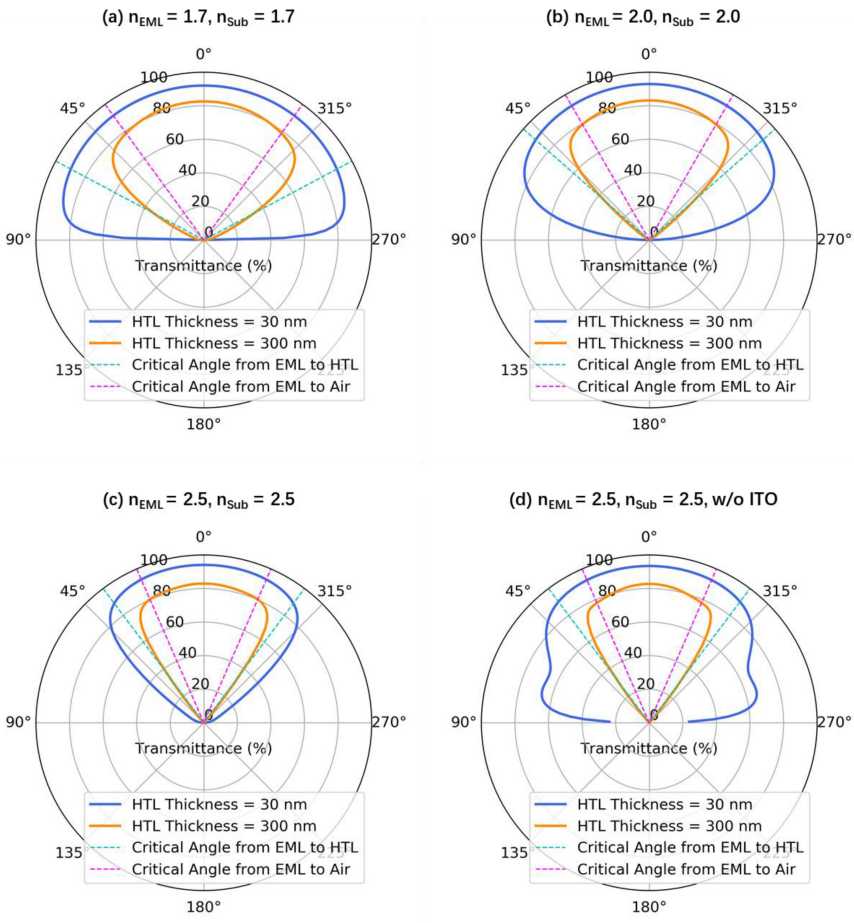

Fig. 8. Emission intensity angular distribution within the substrate and for $\lambda = 530$ nm, and varied refractive indices of (a) $n_{EML} = 1.7$ $n_{Sub} = 1.7$, (b) $n_{EML} = 2.0$ $n_{Sub} = 2.0$, (c) $n_{EML} = 2.5$ $n_{Sub} = 2.5$, (d) $n_{EML} = 2.5$ $n_{Sub} = 2.5$ without ITO.

research has been done on EES like prisms [43], micro-lens array [21], [22], roughened surface [44], [45] on substrates to extract a large fraction of lights from the substrate to air. These methods are not only low cost and convenient, but also avoid interruption of the internal device structure. On the contrary, if optical tunneling is not utilized, the internal extraction structures (IES) may suffer from complicated fabrication, declining electrical behavior, and large area limitation [46]. The wider intensity angular distribution within the substrate suggests that EES will be more effective than IES once the thin HTL and the high-index substrate are applied.

In OLEDs, employing high-index substrates with extraction structures, the EQE can be increased by 2.3 fold experimentally (3 fold theoretically) from 26% to 60% [47], [48]. Different from OLEDs, the refractive index of the emitting layer in QLEDs and PeLEDs is much higher, limiting the efficiency severely [Fig. 1(b)]. However, with the aid of optical tunneling, a similar extraction strategy employing a high-index substrate with extraction structures will bring much improvement in efficiency. If a hemisphere lens with the same index as the substrate is placed on the substrate, almost all the light within the substrate can be extracted to air. This suggests that the upper LEE limit of EES can be increased from 22% to 86% by optimized optical tunneling according to Fig. 7(a).

It is worth mentioning that it is not applicable to discuss optical tunneling in OLEDs in most cases, because common organic polymers as EML only have a refractive index of $\sim$1.7, which

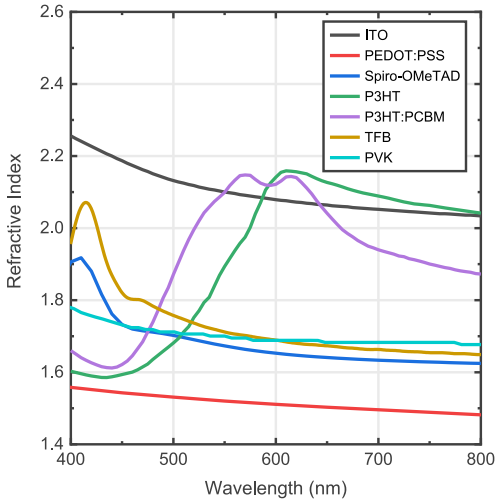

Fig. 9. Refractive index ***n*** of some common electron/hole transport layers.

is well-matched with HTL and the substrate. As for QLEDs and PeLEDs, the "optical tunneling + EES" strategy provides us this special opportunity to unleash the full potential efficiency.

5. Opportunity for Most Devices

As mentioned, the high refractive index EML will severely limit the LEE of the device. Some perovskites even have higher refractive indices than 2, so much light will be reflected by low-index HTL or ETL, indicating that optical tunneling could be utilized. Fig. 9 illustrates the wavelength-dependent refractive indices **n** of some common hole and electron transport layers [27]–[32], [36], [49] (HTL/ETL). In the visible spectrum, most HTL and ETL materials have a lower refractive index than EML and ITO, indicating that optical tunneling followed by EES has extensive suitability in QLED and PeLED. Especially when the EML material has a relatively high refractive index, more attention needs to be paid to optical tunneling and corresponding light extraction strategy.

6. Conclusion

In most of the QLEDs and PeLEDs, there is a large refractive index difference between EML and HTL. This large difference usually causes strong light trapping at the interface of HTL and EML, and thus leads to limited light extraction. Here, we propose an optical tunneling method to extract the light energy which is supposed to be reflected by the HTL and trapped within the device. Taking full advantage of optical tunneling, the trapped light energy is released to the substrate. At this stage, only the simple and widely-known techniques such as a rough glass substrate are needed to release all of the trapped energy to air. In this work, we theoretically demonstrate two to three times enhancement of substrate modes by reducing the thickness of HTL and employing high-index substrates followed the guidance of optical tunneling. The enhanced substrate modes suggest the external light extraction structure can significantly enhance LEE. Moreover, the external light extractors are more preferable than the internal light extractors due to the extended intensity angular distribution within the substrate. We believe optical tunneling followed by EES would be a cost-effective strategy to achieve high LEE in QLEDs and PeLEDs.

References

[1] Y. Shirasaki, G. J. Supran, M. G. Bawendi, and V. Bulović, "Emergence of colloidal quantum-dot light-emitting technologies," *Nat. Photon.*, vol. 7, no. 1, pp. 13–23, 2013.
[2] B. R. Sutherland and E. H. Sargent, "Perovskite photonic sources," *Nat. Photon.*, vol. 10, no. 5, pp. 295–302, 2016.
[3] H. Shen *et al.*, "Visible quantum dot light-emitting diodes with simultaneous high brightness and efficiency," *Nat. Photon.*, vol. 13, no. 3, pp. 192–197, 2019.
[4] K. Lin *et al.*, "Perovskite light-emitting diodes with external quantum efficiency exceeding 20 per cent," *Nature*, vol. 562, no. 7726, pp. 245–248, 2018.
[5] J.-I. Shim and D.-S. Shin, "Measuring the internal quantum efficiency of light-emitting diodes: Towards accurate and reliable room-temperature characterization," *Nanophotonics*, vol. 7, no. 10, pp. 1601–1615, 2018.
[6] B. S. Mashford *et al.*, "High-efficiency quantum-dot light-emitting devices with enhanced charge injection," *Nat. Photon.*, vol. 7, no. 5, pp. 407–412, 2013.
[7] Y. Fang, Q. Dong, Y. Shao, Y. Yuan, and J. Huang, "Highly narrowband perovskite single-crystal photodetectors enabled by surface-charge recombination," *Nat. Photon.*, vol. 9, no. 10, pp. 679–686, 2015.
[8] A. Salehi, Y. Chen, X. Fu, C. Peng, and F. So, "Manipulating refractive index in organic light-emitting diodes," *ACS Appl. Materials Interfaces*, vol. 10, no. 11, pp. 9595–9601, 2018.
[9] D. B. Dement, M. Puri, and V. E. Ferry, "Determining the complex refractive index of neat CdSe/CdS quantum dot films," *J. Phys. Chem. C*, vol. 122, no. 37, pp. 21557–21568, 2018.
[10] M. E. Calvo, "Materials chemistry approaches to the control of the optical features of perovskite solar cells," *J. Materials Chem. A*, vol. 5, no. 39, pp. 20561–20578, 2017.
[11] P. Löper *et al.*, "Complex refractive index spectra of $CH_3NH_3PbI_3$ perovskite thin films determined by spectroscopic ellipsometry and spectrophotometry," *J. Phys. Chem. Lett.*, vol. 6, no. 1, pp. 66–71, 2015.
[12] S. Brittman and E. C. Garnett, "Measuring n and k at the microscale in single crystals of $CH_3NH_3PbBr_3$ perovskite," *J. Phys. Chem. C*, vol. 120, no. 1, pp. 616–620, 2016.
[13] J.-S. Park *et al.*, "Electronic structure and optical properties of α-$CH_3NH_3PbBr_3$ perovskite single crystal," *J. Phys. Chem. Lett.*, vol. 6, no. 21, pp. 4304–4308, 2015.
[14] S. K. Tripathy, P. Sarkar, R. Mayengbam, and K. Baishnab, "Cubic methylammonium lead chloride perovskite as a transparent conductor in solar cell applications: An experimental and theoretical study," *Indian J. Pure Appl. Phys. (IJPAP)*, vol. 57, no. 12, pp. 891–899, 2020.
[15] R. K. Singh, R. Kumar, N. Jain, S. R. Dash, J. Singh, and A. Srivastava, "Investigation of optical and dielectric properties of cspbi$_3$ inorganic lead iodide perovskite thin film," *J. Taiwan Inst. Chem. Engineers*, vol. 96, pp. 538–542, 2019.
[16] N. C. Greenham, R. H. Friend, and D. D. Bradley, "Angular dependence of the emission from a conjugated polymer light-emitting diode: Implications for efficiency calculations," *Adv. Materials*, vol. 6, no. 6, pp. 491–494, 1994.
[17] Y. Jiang, S.-Y. Cho, and M. J. J. o. M. C. C. Shim, "Light-emitting diodes of colloidal quantum dots and nanorod heterostructures for future emissive displays," *J. Mater. Chem. C*, vol. 6, no. 11, pp. 2618–2634, 2018.
[18] J. Chen *et al.*, "All solution-processed stable white quantum dot light-emitting diodes with hybrid zno@ TiO_2 as blue emitters," *Scientific Reports*, vol. 4, no. 1, pp. 1–6, 2014.
[19] Y. Shen *et al.*, "High-Efficiency perovskite light-emitting diodes with synergetic outcoupling enhancement," *Adv. Materials*, vol. 31, no. 24, 2019, Art. no. 1901517.
[20] S. Mladenovski, K. Neyts, D. Pavicic, A. Werner, and C. Rothe, "Exceptionally efficient organic light emitting devices using high refractive index substrates," *Opt. Exp.*, vol. 17, no. 9, pp. 7562–7570, 2009.
[21] S. Möller and S. Forrest, "Improved light out-coupling in organic light emitting diodes employing ordered microlens arrays," *J. Appl. Phys.*, vol. 91, no. 5, pp. 3324–3327, 2002.
[22] H. Peng, Y. L. Ho, X.-J. Yu, M. Wong, and H.-S. Kwok, "Coupling efficiency enhancement in organic light-emitting devices using microlens array-theory and experiment," *J. Display Technol.*, vol. 1, no. 2, pp. 278–282, 2005.
[23] T. Yamasaki, K. Sumioka, and T. Tsutsui, "Organic light-emitting device with an ordered monolayer of silica microspheres as a scattering medium," *Appl. Phys. Lett.*, vol. 76, no. 10, pp. 1243–1245, 2000.
[24] H. W. Chang *et al.*, "Organic light-emitting devices integrated with internal scattering layers for enhancing optical out-coupling," *J. Soc. Inf. Display*, vol. 19, no. 2, pp. 196–204, 2011.
[25] Y. Sun and S. R. Forrest, "Enhanced light out-coupling of organic light-emitting devices using embedded low-index grids," *Nat. Photon.*, vol. 2, no. 8, pp. 483–487, 2008.
[26] Q. Zhang *et al.*, "Efficient metal halide perovskite light-emitting diodes with significantly improved light extraction on nanophotonic substrates," *Nat. Commun.*, vol. 10, no. 1, pp. 1–9, 2019.
[27] J. H. Han, D.-H. Kim, and K. C. Choi, "Microcavity effect using nanoparticles to enhance the efficiency of organic light-emitting diodes," *Opt. Exp.*, vol. 23, no. 15, pp. 19863–19873, 2015.
[28] A. A. Alkanoo, T. M. El-Agez, S. A. Taya, and A. Afghjani, "Characterization of PVK polymeric material using rotating polarizer and analyzer ellipsometer with a speed ratio 1:1," *Sci., Technol. Develop.*, vol. 35, no. 1, pp. 16–21, 2016.
[29] A. Alvarez *et al.*, "Polymeric multilayers for integration into photonic devices," *Thin Solid Films*, vol. 433, no. 1-2, pp. 277–280, 2003.
[30] C. Ramsdale and N. C. Greenham, "The optical constants of emitter and electrode materials in polymer light-emitting diodes," *J. Phys. D: Appl. Phys.*, vol. 36, no. 4, 2003, Art. no. L29.
[31] M. Filipič *et al.*, "$CH_3NH_3PbI_3$ perovskite/silicon tandem solar cells: Characterization based optical simulations," *Opt. Exp.*, vol. 23, no. 7, pp. A263–A278, 2015.
[32] A. Ng, K. Cheung, M. Fung, A. Djurišić, and W. Chan, "Spectroscopic ellipsometry characterization of polymer–fullerene blend films," *Thin Solid Films*, vol. 517, no. 3, pp. 1047–1052, 2008.
[33] S. Wang *et al.*, "Enhanced light out-coupling efficiency of quantum dot light emitting diodes by nanoimprint lithography," *Nanoscale*, vol. 10, no. 24, pp. 11651–11656, 2018.

[34] S. Jeon *et al.*, "Perovskite light-emitting diodes with improved outcoupling using a high-index contrast nanoarray," *Small*, vol. 15, no. 8, 2019, Art. no. 1900135.
[35] S. Kasap, *Optoelectronics and Photonics: Principles and Practices. Upper Saddle River*, Princeton, NJ, USA: Pearson Education, 2013.
[36] Z. C. Holman *et al.*, "Infrared light management in high-efficiency silicon heterojunction and rear-passivated solar cells," *J. Appl. Phys.*, vol. 113, no. 1, 2013, Art. no. 013107.
[37] S. Zhu, A. Yu, D. Hawley, and R. Roy, "Frustrated total internal reflection: A demonstration and review," *Amer. J. Phys.*, vol. 54, no. 7, pp. 601–607, 1986.
[38] J.-W. Lee *et al.*, "In-situ formed type i nanocrystalline perovskite film for highly efficient light-emitting diode," *ACS Nano*, vol. 11, no. 3, pp. 3311–3319, 2017.
[39] J. Liang *et al.*, "Efficient perovskite light-emitting diodes by film annealing temperature control," *RSC Adv.*, vol. 6, no. 75, pp. 71070–71075, 2016.
[40] R. Chance, A. Prock, and R. Silbey, "Molecular fluorescence and energy transfer near interfaces," *Adv. Chem. Phys*, vol. 37, pp. 1–65, 1978.
[41] P. Yeh, "Matrix formulation for isotropic layered media," *Optical Waves in Layered Media*, New York, NY, USA: Wiley, 1998, ch. 5, pp. 102–114.
[42] J. Lu *et al.*, "Ultrathin PEDOT: PSS enables colorful and efficient perovskite light-emitting diodes," *Adv. Sci.*, 2020, Art. no. 2000689.
[43] H.-Y. Lin *et al.*, "Improvement of the outcoupling efficiency of an organic light-emitting device by attaching microstructured films," *Opt. Commun.*, vol. 275, no. 2, pp. 464–469, 2007.
[44] J. Zhou *et al.*, "Roughening the white OLED substrate's surface through sandblasting to improve the external quantum efficiency," *Org. Electron.*, vol. 12, no. 4, pp. 648–653, 2011.
[45] D.-Y. Zhou, X.-B. Shi, C.-H. Gao, S.-D. Cai, Y. Jin, and L.-S. Liao, "Light extraction enhancement from organic light-emitting diodes with randomly scattered surface fixture," *Appl. Surf. Sci.*, vol. 314, pp. 858–863, 2014.
[46] Y. Jiang, S. Chen, G. Li, H. Li, and H. S. Kwok, "A low-cost Nano-modified substrate integrating both internal and external light extractors for enhancing light out-coupling in organic light-emitting diodes," *Adv. Opt. Materials*, vol. 2, no. 5, pp. 418–422, 2014.
[47] A. Mikami and T. Koyanagi, "60.4 L: Late-news paper: High efficiency 200-lm/W green light emitting organic devices prepared on high-index of refraction substrate," in *Proc. SID Symp. Dig. Tech. Papers*, 2009, pp. 907–910.
[48] G. Gaertner and H. Greiner, "Light extraction from OLEDs with (high) index matched glass substrates," in *Proc. Org. Optoelectronics Photon. III*, 2008, Art. no. 69992T.
[49] F. Monestier *et al.*, "Modeling the short-circuit current density of polymer solar cells based on P_3HT: PCBM blend," *Sol. Energy Mater. Sol. Cells*, vol. 91, no. 5, pp. 405–410, 2007.